Pergamon

J. Mech. Phys. Solids, Vol. 45, No. 5, pp. 763–787, 1997

0022–5096/97 $17.00+0.00

PII: S0022–5096(96)00095–6

CRACK BRIDGING IN FIBER REINFORCED CEMENTITIOUS COMPOSITES WITH SLIP-HARDENING INTERFACES

ZHONG LIN and VICTOR C. LI

Advanced Civil Engineering Materials Research Laboratory, Department of Civil and Environmental Engineering, University of Michigan, Ann Arbor, MI 48109, U.S.A.

(*Received* 23 *March* 1996; *in revised form* 20 *August* 1996)

ABSTRACT

A new crack bridging model accounting for slip-hardening interfacial shear stress is derived for randomly oriented discontinuous flexible fibers in cement-based composites, based on a micromechanics analysis of single fiber pull-out. The complete composite bridging stress versus crack opening curve (σ_B–δ relation) and associated fracture energy are theoretically determined. A micromechanics-based criterion which governs the existence of post-debonding rising branch of the σ_B–δ curve is obtained. Implications of the present model on various composite properties, including uniaxial tensile strength, flexural strength, ductility and critical fiber volume fraction for strain-hardening, are discussed together with an example of a 2% polyethylene fiber reinforced cement composite. It is found that the present model can very well describe the slip-hardening behavior during fiber pull-out which originates from fiber surface abrasion at fiber/matrix interface. In addition, the new model predicts accurately the enhanced toughness in terms of both ultimate tensile strain and fracture energy of the composite and resolves the deficiency of constant interface shear stress model in predicting the crack opening and ultimate strain, which are critical for material design of pseudo strain hardening engineered cementitious composites (ECCs).

Keywords: A. fracture toughness, A. ductility, B. fiber-reinforced composite material, B. concrete, slip-hardening interface.

1. INTRODUCTION

Introduction of fibers in a cement-based matrix can significantly increase the failure strain and fracture toughness of the composite by orders of magnitude (e.g., Krenchel and Hansen, 1987; Naaman, 1992; Li *et al.*, 1995a; Maalej *et al.*, 1995). The underlying mechanism is that fibers undergo debonding and sliding against matrix and stabilize matrix cracks by exerting closure traction on the crack surfaces (Aveston *et al.*, 1971; Marshall *et al.*, 1985; McCartney, 1987; Hutchinson and Jensen, 1990; Li, 1992). If properly designed, intact bridging fibers can transfer sufficient load after first cracking to allow the composite to undergo multiple cracking and show strain-hardening behavior (e.g., Li and Leung, 1992; Li and Wu, 1992). Figure 1(a) shows general features of the uniaxial tensile stress–strain relation of such a strain-hardening cementitious material compared to brittle and quasi-brittle materials (e.g., plain concrete or ordinary fiber reinforced concrete (FRC)). Three typical deformation

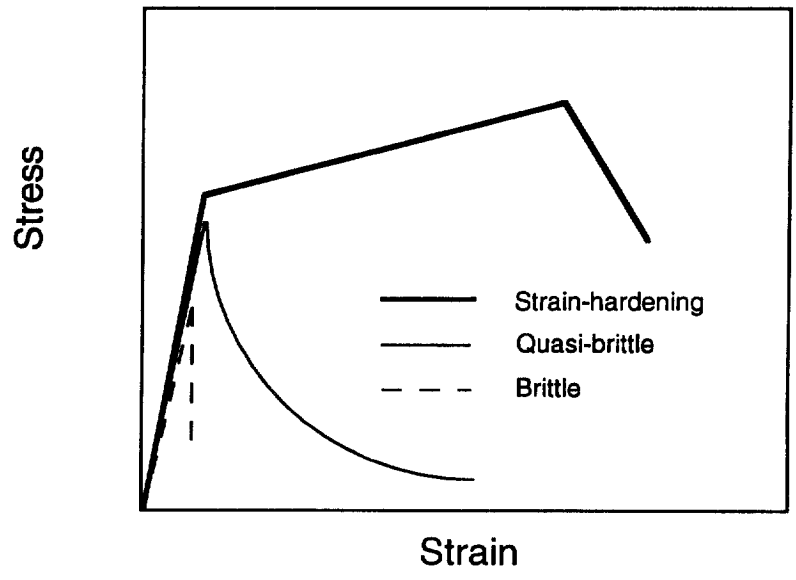

(a)

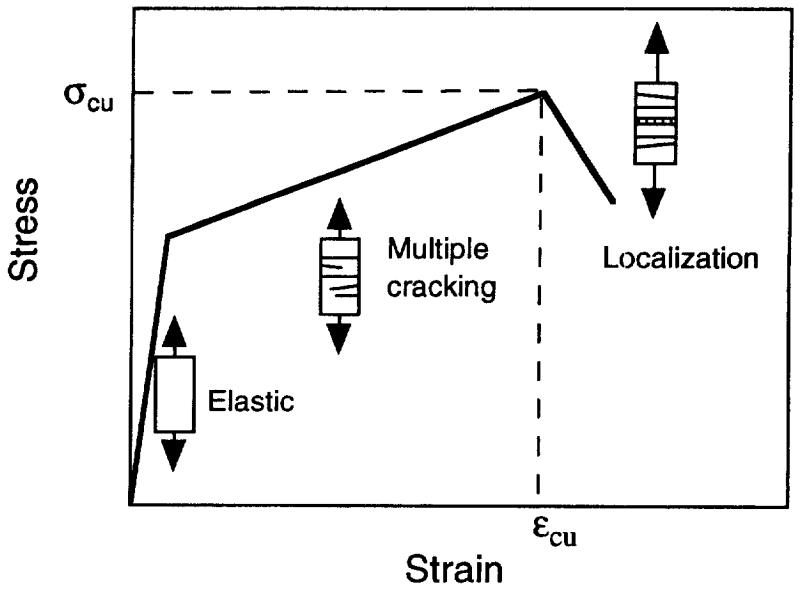

(b)

Fig. 1. (a) Schematic illustration of uniaxial tensile stress–strain curves for brittle, quasi-brittle and strain-hardening cementitious materials. (b) Schematic of three deformation stages of a strain-hardening cementitious composite during a uniaxial tensile test.

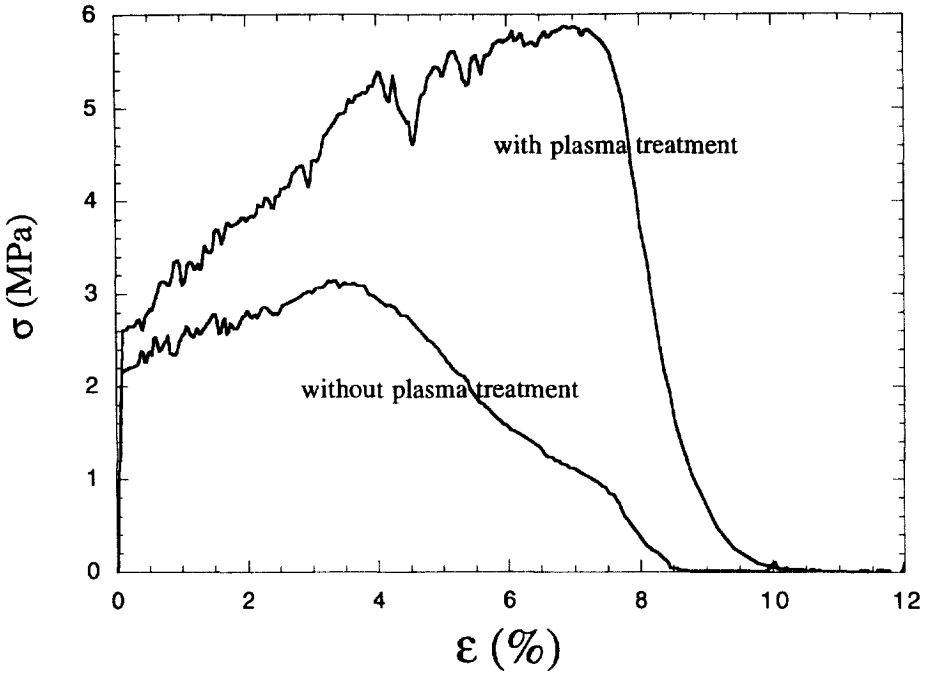

Fig. 2. Tensile stress–strain curves of 2% polyethylene fiber (with and without prior argon plasma treatment) reinforced cement matrix composites (after Li *et al.*, 1995a).

stages associated with a uniaxial tensile stress–strain relation of a strain-hardening cementitious composite, namely, elastic deformation, multiple cracking and damage localization, are shown schematically in Fig. 1(b). In fact, the ductility of such an engineered cementitious composite (ECC) is so high that it is more akin to metal than conventional concrete (Fig. 2). The potential of the composite material is best utilized by stable multiple cracking in contrast to catastrophic failure due to single crack propagation in plain concrete or FRCs. A comprehensive review of micromechanical models of mechanical response of high performance fiber reinforced cementitious composites (HPFRCC) was recently provided by Li *et al.* (1995b).

Over the last decade, micromechanical models for fiber reinforced cementitious composite materials have gradually evolved in sophistication so that a structural performance driven material design has been made possible (Li, 1993). The most crucial link between the properties of fiber, matrix and fiber/matrix interface and that of a composite is the crack bridging stress–crack opening relation (σ_B–δ relation). In general, a σ_B–δ relation defines the ultimate stress and strain of a uniaxial tensile stress–strain curve (σ_{cu} and ε_{cu} in Fig. 1(b)) and the energy consumption due to fiber bridging, which in turn control the strength, ductility and fracture toughness of a structural member. Therefore, a reliable stress–strain relation of a composite based on a micromechanical model is needed in order to design a composite material that can meet the performance requirements of a structure.

For randomly oriented discontinuous flexible fiber reinforced cementitious com-

posites, Li (1992) derived a crack bridging model based on constant frictional interface stress (hereafter designated as the constant-τ model). This simple model can predict the postcracking stress–displacement relation and pullout fracture energy experimentally determined for both steel-fiber and synthetic-fiber reinforced cementitious composites of widely varying micromechanical parametric values. However, discrepancies have been observed with this constant-τ model when it comes to those fiber/matrix systems with strong slip-dependent interface behavior, especially for crack opening prediction at maximum bridging stress. In some cases, the constant-τ model predicts much smaller crack opening than that from direct measurement at maximum stress under direct tension for materials with strain-hardening behavior, as can be seen later in this paper. A new crack bridging model that takes into account the slip-dependent interfacial shear stress is needed to resolve this problem.

The phenomenon of slip-dependent interfacial shear stress, namely, the interfacial shear stress depends on the local slippage distance between fiber and matrix, has been suggested by a number of researchers. Wang *et al.* (1988) found that for nylon and polypropylene fibers, it was necessary to have an increasing interfacial shear stress with slippage distance (slip-hardening interface) in order to describe the experimental pull-out curves while for steel fibers, a decreasing τ with slippage distance was needed. Shao *et al.* (1993) used a Moiré interferometry technique to measure the in-plane displacements around the continuous steel fiber/cement matrix interface and they calculated the interface slip and the interface shear stress in the so-called 'break-down' zone where the interface shear stress decayed with increasing value of the slip distance (Li and Stang, 1996). Slip-dependent interface behavior has also been found in aligned continuous fiber reinforced metal and ceramic matrix composites (Yang *et al.*, 1991; Holmes and Cho, 1992). Several crack bridging models were developed by Bao and Song (1993) for these aligned continuous fiber composites. Most recently, Li and Stang (1996) provided a review article on characterization and control of various interface properties, including slip-hardening and softening effects, for discontinuous fiber reinforced cement composites.

In general, the slip-dependent interface shear stress can be attributed to fiber surface abrasion, asperity wear, fragmentation of fiber coatings at the debonded interface, etc. In particular, for synthetic fiber (usually polymeric fiber)/cement matrix composites, fiber abrasion is most likely the mechanism behind slip-hardening interface behavior. Due to the relatively low hardness of polymeric fibers, severe surface abrasion may occur when fibers try to slip against the rough surrounding matrix with higher hardness. Fiber debris, often observed in the form of stripped fibrils, will accumulate at the debonded interface as slippage increases and create a 'jamming' effect to make fiber slipping more difficult and hence increases the interface shear stress.

In this paper, we will focus on discontinuous synthetic fiber/cement matrix systems. A simple interface constitutive relationship is adopted to quantify the slip-hardening interface behavior. Theoretical models for single fiber pull-out curves are then constructed with comparison to experimental results of polyethylene fibers (Spectra 900). A crack bridging model accounting for random fiber orientation, fiber snubbing effect and slip-hardening interfacial shear stress is derived based on the interface constitutive relation and a micromechanical model for single fiber pull-out. Implications of this

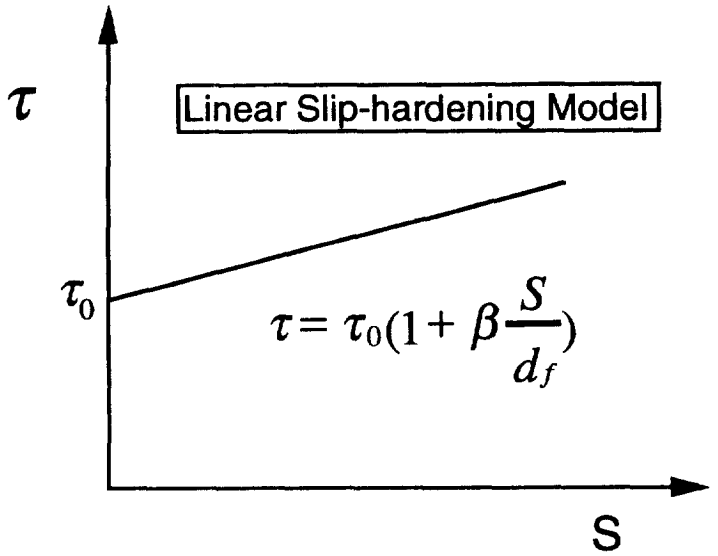

Fig. 3. Linear slip-hardening interface constitutive relation.

crack bridging model are discussed along with an example of a 2% polyethylene/cement composite to illustrate the effects of slip-hardening interface behavior on various properties of the composite material. Conclusions are drawn at the end of this paper.

2. INTERFACE CONSTITUTIVE RELATIONSHIP

To characterize the slip-hardening interface behavior, a model relating interface shear stress τ and interface slip S (relative displacement between fiber and matrix) must be developed. Equation (1) is a general form of such a relation where both τ and S should be understood as functions of position along the interface when slip is non-uniform as in the case of a fiber bridging across a matrix crack.

$$\tau = \tau(S). \tag{1}$$

For simplicity, a simple two-parameter phenomenological model proposed by Bao and Song (1993) is adopted, which describes a linear dependence between τ and S as follows

$$\tau = \tau_0(1 + \beta S/d_f) \tag{2}$$

where τ_0 is the frictional sliding shear stress at the tip of debonding zone where no slip occurs ($S = 0$), β is a nondimensional hardening parameter and d_f is fiber diameter. Figure 3 illustrates this so-called linear hardening model. The constant-τ model ($\beta = 0$) is a special case of (2). Both τ_0 and β need to be determined empirically either by curve-fitting a single fiber pull-out P–δ curve (Wang *et al.*, 1988) or by direct measurement using Moiré interferometry (Shao *et al.*, 1993). Calibration of these two

parameters from a single fiber pullout test will be discussed in the next section. It should be noted that (2) is the building block for our subsequent theoretical modeling. τ_0 and β will enter the crack bridging model as basic micromechanical parameters which control the mechanical properties of the composite material. It should be made clear that τ_0 and β represent the constitutive behavior of a fiber/matrix interface and they should not change with different experimental set-ups. Equation (2) may require additional higher order terms (Wang *et al.*, 1988) to describe a complete single fiber pullout curve very accurately. However, given the practical crack opening in the order of sub-millimeter in a composite, the initial rising portion after the fiber is fully debonded is the most important (as will be seen shortly), and (2) will be sufficient.

3. SINGLE FIBER PULLOUT

Consider an isolated fiber loaded at its end with a force P resisted by a slip-dependent interfacial shear stress τ (e.g. equation (2)) at its interface along its length L embedded in a cement matrix (Fig. 4). The fiber and the matrix are taken as elastic, with Young's modulus E_f and E_m respectively; the effect of Poisson's ratio and the elastic bond between fiber and matrix are neglected. The fiber, with diameter d_f, is assumed to be frictionally bonded to the matrix, and thus debonding of the fiber should be understood as the activation of interfacial frictional slip. Before debonding reaches the embedded end of the fiber, the entire fiber/matrix interface is divided into two regions: the intact region and the debond/slid region with length ℓ. As load P increases, ℓ increases. Complete debonding occurs when ℓ reaches its maximum value L, the fiber embedment length. Then the fiber is assumed to be pulled out of the matrix without rupture in a rigid manner, meaning the elastic stretch of the fiber compared to the fiber end displacement during the pullout stage is negligible. It can be shown that the relation between load P and the displacement of the loaded-end of the fiber is given by (Appendix I)

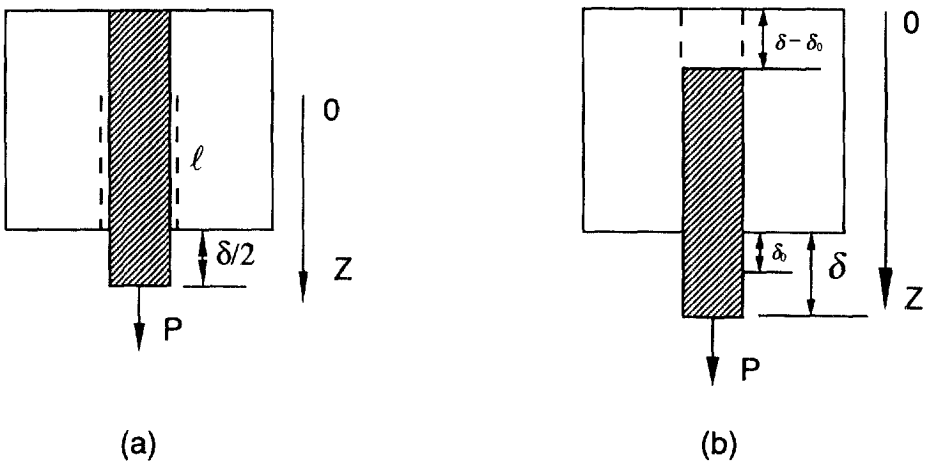

Fig. 4. Schematic of fiber debonding (a), and pullout (b).

$$P = \frac{\pi d_f^2 \tau_0 (1+\eta)}{\omega} \sqrt{\left(1 + \frac{\beta\delta}{2d_f}\right)^2 - 1}, \quad \text{for } 0 \leqslant \delta \leqslant \delta_0 \tag{3}$$

for the fiber debonding stage, and

$$P = \frac{\pi d_f^2 \tau_0 (1+\eta)}{\omega} \left[\sinh\left(\frac{\omega L}{d_f}\right) - \sinh\left(\frac{\omega(\delta - \delta_0)}{d_f}\right) \right] + \pi \tau_0 \beta (1+\eta)(\delta - \delta_0)(L - (\delta - \delta_0)) \tag{4}$$

for the fiber pullout stage ($\delta_0 < \delta \leqslant L$), where

$$\eta = \frac{V_f E_f}{V_m E_m}, \quad \omega = \sqrt{4(1+\eta)\beta\tau_0 / E_f},$$
$$\delta_0 = \frac{2d_f}{\beta} \left[\cosh\left(\frac{\omega L}{d_f}\right) - 1 \right] \tag{5}$$

and $P = 0$ for $\delta > L$. V_f and V_m are the volume fractions of fiber and matrix, respectively. δ_0 corresponds to the displacement at which debonding is completed along the full length of the embedded fiber segment.

To examine the validity of (3) and (4) for a fiber/matrix system with slip-hardening interface behavior, experimental single fiber pull-out curves for polyethylene fibers, both with and without plasma treatment, in a cement matrix, are plotted in Fig. 5 along with theoretical predictions of (3) and (4). Plasma treatment of the fiber modifies the surface reactivity and wettability between the fiber and cement (Li *et al.*, 1996). As can be seen from the experimental results shown in Fig. 5, plasma treatment also increases the rate of slip-hardening (indicated by a steeper slope after the first bend-over point). The two parameters τ_0 and β are obtained by the following procedures: (a) use the load at first bend-over point (full debonding point) to obtain τ_0 since the fiber slip is usually small up to full debonding point ($\delta < \delta_0 \sim 10^1$ μm) and the influence of β is negligible; (b) with τ_0 fixed, adjust β (usually of order 10^{-3} to 10^{-2} for synthetic fiber/cement matrix systems) to match the slope of the pullout curve after the first bend-over point; (c) further fine-tuning may be needed to achieve a best fit. Clearly, as can be seen from Fig. 5, the theoretical model can capture the key features of a single fiber pullout curve. When displacement is large (after the load reaches maximum value), the theoretical curves start to deviate from the experimental data due to the possibility of saturation of slip-hardening. On the other hand, the constant-τ model is clearly not suitable for describing the P–δ relation of these fiber/matrix systems due to its inherent deficiency of not taking into account the change in interfacial shear stress during fiber pullout.

Equations (3) and (4) are for fibers pulled out in a direction along the fiber axis. For nonaligned fibers, as in randomly distributed discontinuous fiber reinforced cementitious composites, various studies have indicated an angle effect on the pullout load P. For flexible (in bending, dependent on elastic stiffness and fiber diameter) steel and polymeric fibers, Morton and Groves (1976) and Li *et al.* (1990) found an

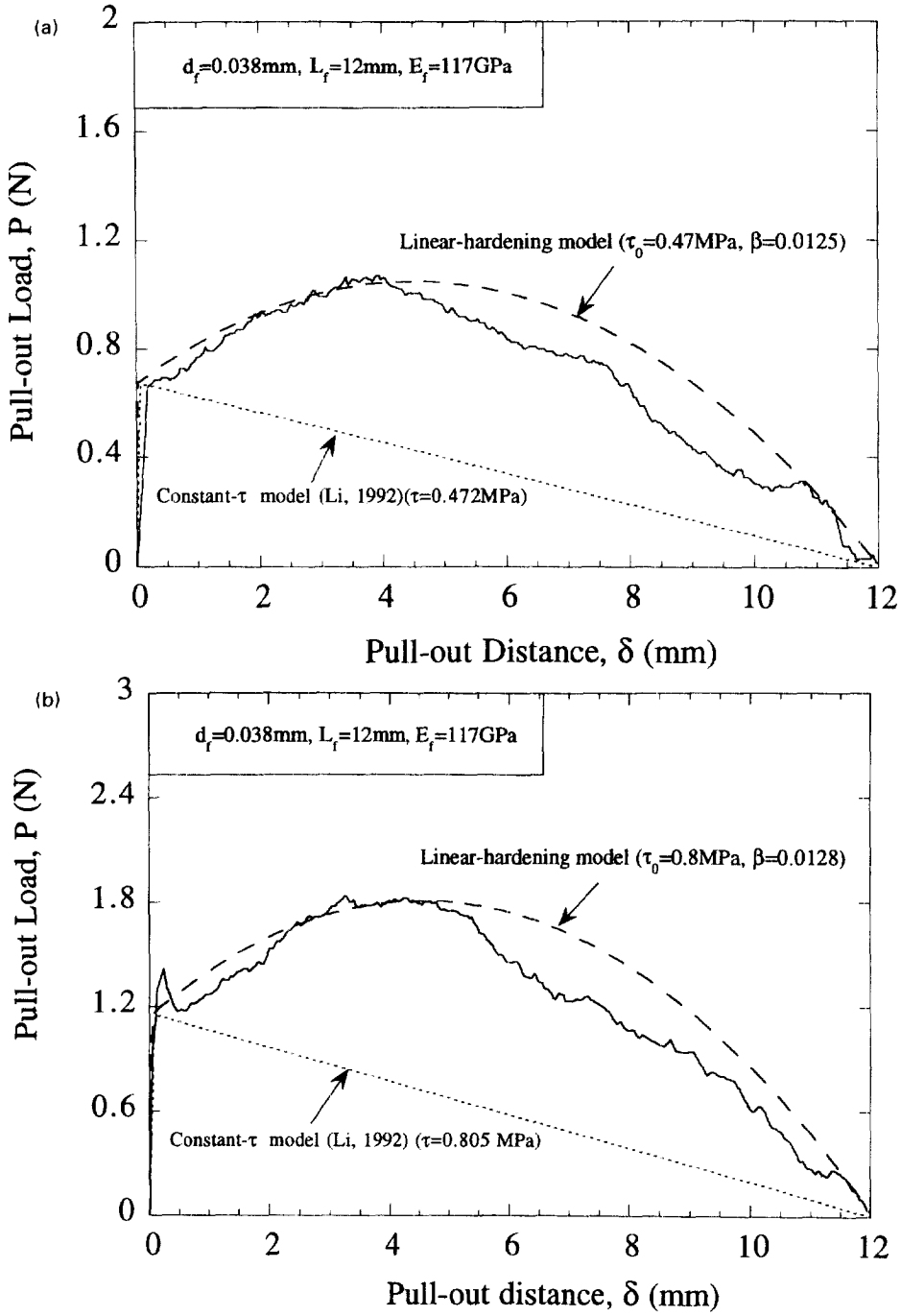

Fig. 5. Predictions by slip-hardening single fiber pullout model (3) and (4) (with $\eta = 0$) in comparison with experimental results (from Li *et al.*, 1995a) and the constant-τ model (Li, 1992): (a) spectra 900 fiber without plasma treatment, and (b) the same fiber with plasma treatment.

increase of P with angle ϕ of inclination of fiber to the loading axis. This snubbing effect could be incorporated into the pullout force P by recognizing

$$P(\delta;\phi) = P(\delta;\phi=0)e^{f\phi} \tag{6}$$

where f is a snubbing coefficient and can be experimentally determined. Experimental tests of fiber pullout at inclined angles up to 80 degrees suggest f-values of 0.7 and 0.9 for nylon and polypropylene fibers embedded in a normal-strength mortar matrix.

4. CRACK BRIDGING MODEL

For a composite with randomly distributed discontinuous fibers of volume fraction V_f, Li *et al.* (1991) showed that the composite σ_B–δ curve can be predicted by averaging over the contributions of *only* those individual fibers that cross the matrix crack plane:

$$\sigma_B(\delta) = \frac{4V_f}{\pi d_f^2}\int_{\phi=0}^{\pi/2}\int_{z=0}^{(L_f/2)\cos\phi} P(\delta)p(\phi)p(z)\,dz\,d\phi \tag{7}$$

where $p(\phi)$ and $p(z)$ are the probability density functions of the orientation angle and centroidal distance of fibers from the crack plane, respectively. For uniform random distributions, $p(\phi) = \sin\phi$, and $p(z) = 2/L_f$ (Li *et al.*, 1991).

For composites with linear slip-hardening interfaces, using (3)–(6) in (7), we find (Appendix II) that the σ_B–δ relation is given by

$$\frac{\sigma_B}{\sigma_0} = \begin{cases} \dfrac{2}{k}\left\{\left[1-\dfrac{1}{k}\cosh^{-1}\left(1+\lambda\dfrac{\tilde\delta}{\tilde\delta^*}\right)\right]\sqrt{\left(1+\lambda\dfrac{\tilde\delta}{\tilde\delta^*}\right)^2-1}+\dfrac{\lambda}{k}\dfrac{\tilde\delta}{\tilde\delta^*}\right\} & (0\le\tilde\delta\le\tilde\delta^*) \\ \left(1+\dfrac{\beta L_f}{2d_f}\tilde\delta\right)(1-\tilde\delta)^2 & (\tilde\delta^*<\tilde\delta\le 1) \\ 0 & (\tilde\delta>1) \end{cases} \tag{8a, b, c}$$

where

$$\sigma_0 = \tfrac{1}{2}g\tau_0 V_f(1+\eta)L_f/d_f, \tag{9}$$

$$k = \omega L_f/(2d_f); \quad \lambda = \cosh(k)-1, \tag{10}$$

$$\tilde\delta = \delta/(L_f/2), \quad \tilde\delta^* = \frac{2d_f}{\beta}[\cosh(k)-1]/(L_f/2) \tag{11}$$

and g is the snubbing factor related to the snubbing coefficient f by

$$g = \frac{2}{4+f^2}(1+e^{\pi f/2}). \tag{12}$$

Since $\tilde\delta^*$ is the crack opening (normalized by $L_f/2$) at which all fibers have completed

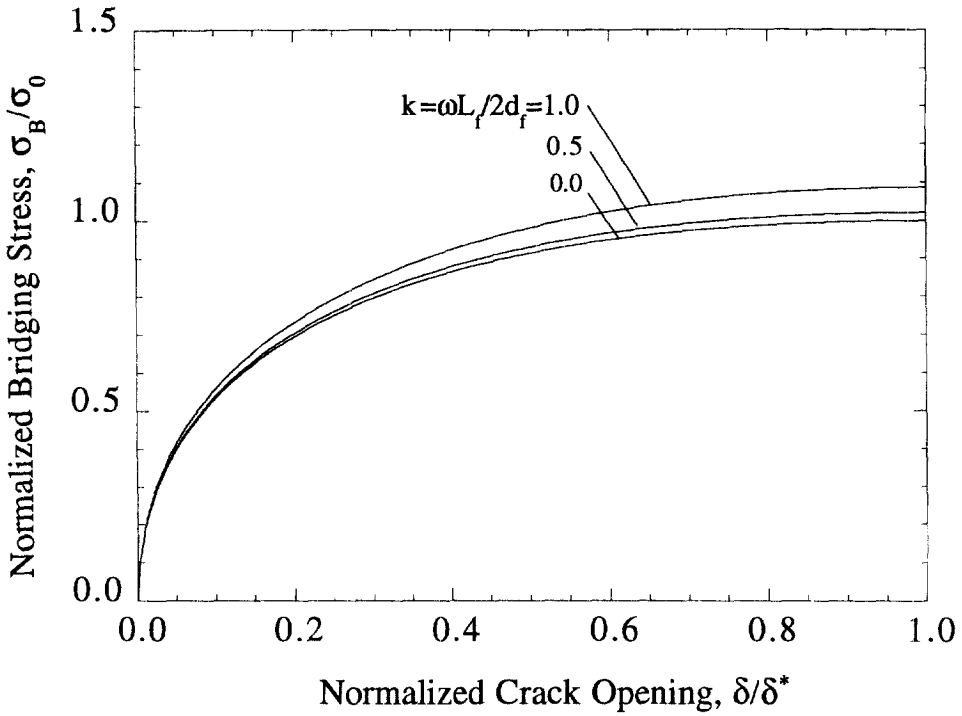

Fig. 6. Pre-debonding crack bridging relation predicted by (8a). $k = 0$ indicates the special case of constant interfacial shear stress ($\tau = \tau_0$).

debonding from the matrix, we shall denote the first equation in (8) as pre-debonding relation and the second one as post-debonding or pullout relation. Plotted in Fig. 6 is the pre-debonding relation with various k values; $k = 0$ corresponds to the constant-τ case. For most synthetic fiber/cement matrix systems, k is less than 10^{-1} ($\tau_0/E_f \sim 10^{-4}$, $\beta \sim 10^{-2}$, $\omega \sim 10^{-3}$, and $L_f/d_f \sim 10^2$); hence, the effect of slip-hardening is negligible at pre-debonding stage. This is due to very small slippage that fibers experienced during this stage. On the other hand, the effect of slip-hardening will become more pronounced during pullout stage since fibers undergo large slippage relative to the matrix. It is indeed the case as shown in Fig. 7. The single controlling parameter in this post-debonding relation is $\beta L_f/(2d_f)$, which is a combination of slip-hardening coefficient and fiber aspect ratio. As indicated by Fig. 7, there is a transition value of $\beta L_f/(2d_f)$ beyond which the normalized post-debonding crack bridging relation will show a rising branch. This is the most important finding in the present work.

Physically, the critical value of $\beta L_f/(2d_f)$ governing the existence of a rising branch of the post-debonding crack bridging relation reflects the trade-off between two competing effects: slip-hardening induced load increase and fiber pullout induced load decrease. In addition to a sufficiently large slip-hardening coefficient β, in order to have a net increase in bridging stress, fibers should be long enough to have large enough slippage (and hence interfacial shear stress) before complete pullout to

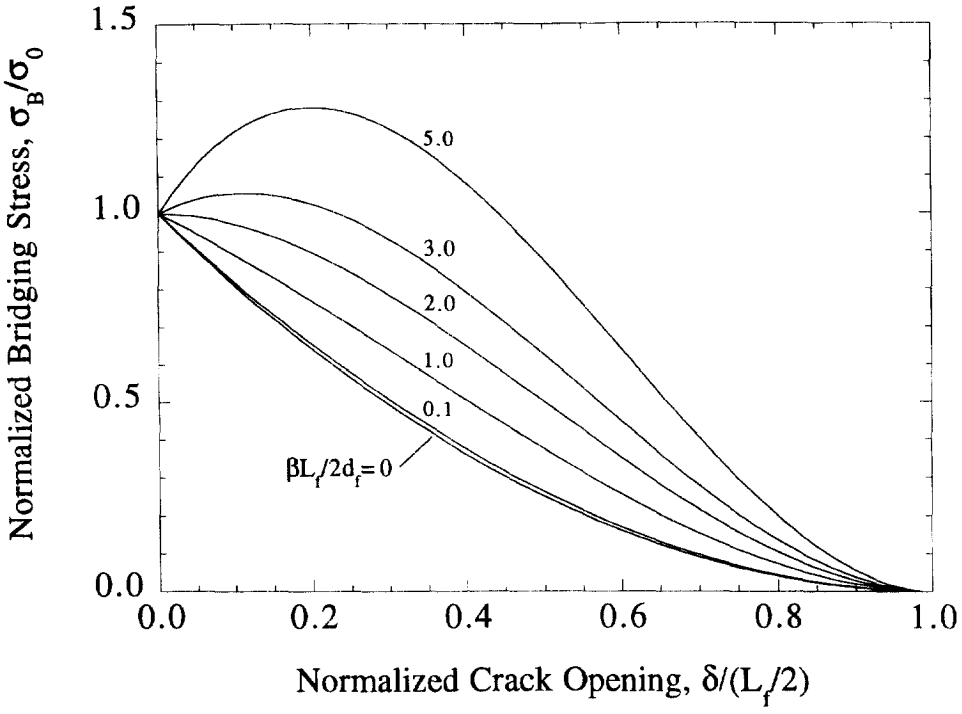

Fig. 7. Post-debonding crack bridging relation predicted by (8b). The curves start to show a rising portion beyond a certain value of $\beta L_f/(2d_f) \approx 2$.

overcome the loss in bridging stress due to decreasing fiber/matrix contact area during pullout. As will become clear shortly, the post-debonding rising branch of the present crack bridging law has significant influence on the ultimate tensile stress and strain, maximum crack opening at ultimate tensile stress, fracture energy as well as the critical fiber volume fraction for multiple cracking to occur in a randomly distributed fiber reinforced cementitious composite.

5. IMPLICATIONS OF THE PRESENT CRACK BRIDGING MODEL

5.1. *Composite ultimate tensile stress and strain*

As pointed out in the last section, there exists a critical value of $\beta L_f/(2d_f)$ beyond which the post-debonding crack bridging relation will show a rising portion. To determine this critical value, consider the second equation in (8) and take the derivative with respect to $\tilde{\delta}$. By setting $d\tilde{\sigma}_B/d\tilde{\delta} = 0$, we have

$$\tilde{\delta}_1 = \frac{c-2}{3c} \quad \text{with } c = \beta L_f/(2d_f) \tag{13}$$

and for post-debonding,

$$\tilde{\delta}_1 > \tilde{\delta}^*. \tag{14}$$

Combining (13) and (14), we obtain

$$c = \frac{\beta L_f}{2d_f} > \frac{2}{1-3\tilde{\delta}^*} \approx 2 \quad (\tilde{\delta}^* \ll 1) \tag{15}$$

which is the condition for a rising portion of the post-debonding crack bridging curve to exist, and it is envisioned in Fig. 7.

After the first matrix crack runs through the entire cross-section of a tensile specimen, the tensile stress is controlled by the bridging stress. Based on (8) through (15), the ultimate tensile stress is given by

$$\sigma_{cu} = \frac{2\lambda}{k^2}\sigma_0, \quad \text{for } \frac{\beta L_f}{2d_f} < 2 \tag{16}$$

and

$$\sigma_{cu} = \left(1 + \frac{\beta L_f}{2d_f}\tilde{\delta}_1\right)(1-\tilde{\delta}_1)^2\sigma_0, \quad \text{for } \frac{\beta L_f}{2d_f} > 2. \tag{17}$$

For strain-hardening cementitious composite materials, multiple cracking and associated crack opening give rise to large ultimate strain. By assuming uniform crack spacing and crack opening at maximum tensile stress, the associated overall tensile strain is given by

$$\varepsilon_{cu} = \frac{\delta_{cu}}{x_d} \tag{18}$$

where δ_{cu} is the maximum crack opening at maximum bridging stress, and it is given by

$$\delta_{cu} = \begin{cases} \dfrac{L_f}{2}\tilde{\delta}, & \text{for } \dfrac{\beta L_f}{2d_f} < 2 \\ \dfrac{L_f}{2}\tilde{\delta}_1, & \text{for } \dfrac{\beta L_f}{2d_f} > 2 \end{cases}. \tag{19}$$

Here, x_d is the saturation crack spacing at ultimate tensile stress and can be determined by (Wu and Li, 1992)

$$x_c = \frac{L_f - \sqrt{L_f^2 - 2\pi\psi L_f x}}{2} \tag{20}$$

where

$$\psi = \frac{4}{\pi g}, \quad x = \frac{V_m \sigma_{mu} d_f}{4 V_f \tau}. \tag{21}$$

In (21), σ_{mu} is the matrix cracking stress and τ should be understood as the average interfacial shear stress obtained from the load at complete debonding on a single fiber pullout curve in the case of slip-hardening.

5.2. *Composite fracture energy*

The fracture energy due to fiber pullout can be calculated from

$$G_c = \int_0^{L_f/2} \sigma_B(\delta)\, d\delta \tag{22}$$

and with σ_B given by (8b), it can be shown that

$$G_c = \frac{1}{12} g\tau_0 V_f (1+\eta) d_f \left(\frac{L_f}{d_f}\right)^2 \left[1 + \frac{1}{4}\left(\frac{\beta L_f}{2d_f}\right)\right]. \tag{23}$$

The second term in (23) is the contribution from slip-hardening, which can be significant when $\beta L_f/2d_f$ is of the order 1.

Energy is also absorbed in the debonding process. This part of the fracture energy may be estimated by integrating the pre-debonding bridging law (8a) and it is usually of the order of $\sigma_0\delta^*$, which is negligibly small compared to the post-debonding fracture energy.

5.3. *Critical fiber volume fraction for multiple cracking*

It has been shown by Marshall *et al.* (1985) and Li and Leung (1992) that, after matrix cracking reaches steady state, the energy needed to propagate the crack is the complimentary energy associated with the crack bridging relation, i.e.,

$$\sigma_{ss}\delta_{ss} - \int_0^{\delta_{ss}} \sigma_B(\delta)\, d\delta = J_c \tag{24}$$

where σ_{ss} and δ_{ss} are the steady state bridging stress and corresponding crack opening, respectively. J_c is the composite critical fracture energy. In order to realize multiple cracking, the steady state bridging stress should not exceed the maximum bridging stress σ_{cu}; otherwise, the composite would have failed upon the first matrix cracking before any other cracks developed. This condition can be expressed as

$$\sigma_{cu} \geqslant \sigma_{ss}. \tag{25}$$

From (8), (16), (17), (24) and (25), it can be shown that the minimum (critical) fiber volume fraction for pseudo strain-hardening behavior of a composite can be approximated by

$$V_f^{crit} = \frac{2J_c}{g\tau_0(1+\eta)(L_f^2/d_f)\Omega} \tag{26}$$

where

$$\Omega = \frac{\lambda}{c}\left(\frac{3\lambda}{k^2} - \frac{4\sqrt{2\lambda}}{3k}\right), \quad \text{for } c = \frac{\beta L_f}{2d_f} < 2 \tag{27}$$

and

$$\Omega = \frac{1}{2}\left[\frac{4}{27}(1+c)(1+1/c)^2\tilde{\delta}_1 - \frac{\lambda}{k^2}\left(\frac{8k}{3\sqrt{2\lambda}} - 1\right)\tilde{\delta}^* - F(\tilde{\delta}_1, \tilde{\delta}^*, c)\right], \quad \text{for } c > 2 \tag{28}$$

with

$$F(\tilde{\delta}_1, \tilde{\delta}^*, c) = \frac{c}{4}(\tilde{\delta}_1 - \tilde{\delta}^*)^4 + \frac{1-2c}{3}(\tilde{\delta}_1 - \tilde{\delta}^*)^3 + \frac{c-2}{2}(\tilde{\delta}_1 - \tilde{\delta}^*)^2 + (\tilde{\delta}_1 - \tilde{\delta}^*). \tag{29}$$

In deriving (26)–(29), (8a) has been simplified as

$$\frac{\sigma_B}{\sigma_0} = \frac{2\lambda}{k^2}\left[\frac{2k}{\sqrt{2\lambda}}\left(\frac{\tilde{\delta}}{\tilde{\delta}^*}\right)^{1/2} - \left(\frac{\tilde{\delta}}{\tilde{\delta}^*}\right)\right] \tag{30}$$

provided $\lambda \sim k^2 \ll 1$, which is generally true for commonly-used synthetic fiber/cement systems. It can be expected that the critical volume fraction required for multiple cracking will drop as the slip-hardening effect becomes stronger because the maximum available complimentary energy is higher for a given fiber volume fraction due to the existence of the post-debonding rising branch of the crack bridging curve. This trend will be illustrated by an example material—polyethylene fiber (Spectra 900)/cement system.

6. AN EXAMPLE—SPECTRA 900 ECC

As indicated by the single fiber pullout tests (Fig. 5), Spectra 900 fiber/cement interface shows strong slip-hardening behavior. The mechanical properties of a composite made of randomly distributed Spectra fibers in a cement matrix (SPECC) are expected to be influenced by its interfacial properties. A micromechanics tool used to predict the composite properties from its interface properties is the crack bridging model developed in this work. In this section, various theoretical and numerical predictions are made using the present bridging model, including composite ultimate tensile stress and strain, crack opening at ultimate tensile stress, critical fiber volume fraction, and flexural stress of a cracked SPECC beam. Comparisons with experimental results are also documented whenever possible.

Table 1 shows the various properties of the fiber and fiber/matrix interface used in our predictions. Additional parameters used are: $E_m = 25$ MPa, $K_m = 0.33$ MPa$\sqrt{\text{m}}$, $\sigma_{mu} = 2.2$ MPa, and $g = 2$. It should be noted that this particular Spectra

Table 1. *Fiber and interface properties of Spectra 900 ECCs*

Fiber	L_f (mm)	d_f (μm)	E_f (GPa)	β	τ_0 (MPa)	$\bar{\tau}$ (MPa)	$\beta L_f/2d_f$
Untreated	12.7	38	117	0.0125	0.48	0.482	2.09
Plasma-treated	12.7	38	117	0.0128	0.8	0.805	2.14

Note: $\bar{\tau} = \tau_0 \sinh(\omega L_f/d_f)/(\omega L_f/d_f)$ from (I.6) and (I.17) in Appendix I.

Table 2. *Model predictions vs experimental results for Spectra 900 ECCs*

	SPECC (untreated)			SPECC (plasma treated)		
	σ_{cu} (MPa)	δ_{cu} (μm)	ε_{cu} (%)	σ_{cu} (MPa)	δ_{cu} (μm)	ε_{cu} (%)
Constant-τ-model	3.2	16	0.6	5.4	27	1.8
Present model	3.5	90	3.3	5.9	137	9.6
Experiment	3.1*	60†	3.5*	5.7*	123†	7.0*

*Data taken from Li *et al.* (1995a).
†Measured by the method used in Wu and Li (1995).

fiber has very high tensile strength such that, for the fiber length (12.7 mm) used, it will always be pullout in the crack wake instead of rupture. The present bridging model is valid for this fiber/matrix system. Values for β and τ_0 are obtained from Fig. 5. The values of $\beta L_f/2d_f$ for both systems are above the critical value 2, indicating slip-hardening interfaces will have significant effect on composite properties.

Table 2 shows the model predictions for composite ultimate stress, strain and associated crack opening under uniaxial tension. Both constant-τ model and the present linear slip-hardening model can predict the ultimate tensile stress reasonably well. However, when it come to crack opening and ultimate strain, constant-τ model is clearly not applicable for both materials while the linear slip-hardening model in this study shows good capability of predicting both crack opening and ultimate strain reasonably close to experimental results. It is also clear that slip-hardening at fiber/matrix interface is the mechanism responsible for large crack opening and strain capacity before ultimate stress is reached.

As pointed out in the last section, significant slip-hardening will give rise to an increase in maximum complimentary energy available for steady state crack propagation and hence reduce the critical fiber volume fraction required for multiple cracking (and strain-hardening) of a composite. To gain some insight on this issue, V_f^{crit} is plotted in Fig. 8 against various values of the interface properties β and τ_0 of a Spectra 900/cement system while other mechanical and geometrical properties of the fiber and matrix are fixed. It can be seen from the plot that for a fixed τ_0, V_f^{crit} has little change until β is large enough so that $\beta L_f/2d_f$ reaches 2. After the critical point, V_f^{crit} has a dramatic drop as β continues to increase. This trend implies a possibility of further reducing material cost by enhancing the interface slip-hardening.

Figure 9 shows the difference in numerical prediction of flexural stress of a SPECC beam by using the constant-τ model and the present slip-hardening model. An initial flaw of size a_0 is assumed. As applied load increases, crack grows in a stable manner in this case due to fiber bridging until a maximum load is reached. Thereafter, crack propagation becomes unstable and the beam fails. Details on the numerical scheme used to compute the load vs crack length curve can be found in Cox and Marshall (1991). As can be seen from Fig. 9, slip-hardening model predicts 20% higher maximum flexural stress than constant-τ model. When crack length is small (so is the crack opening), the bridging stress given by both models are almost identical and that is the reason two curves are initially very close to each other. When crack length and

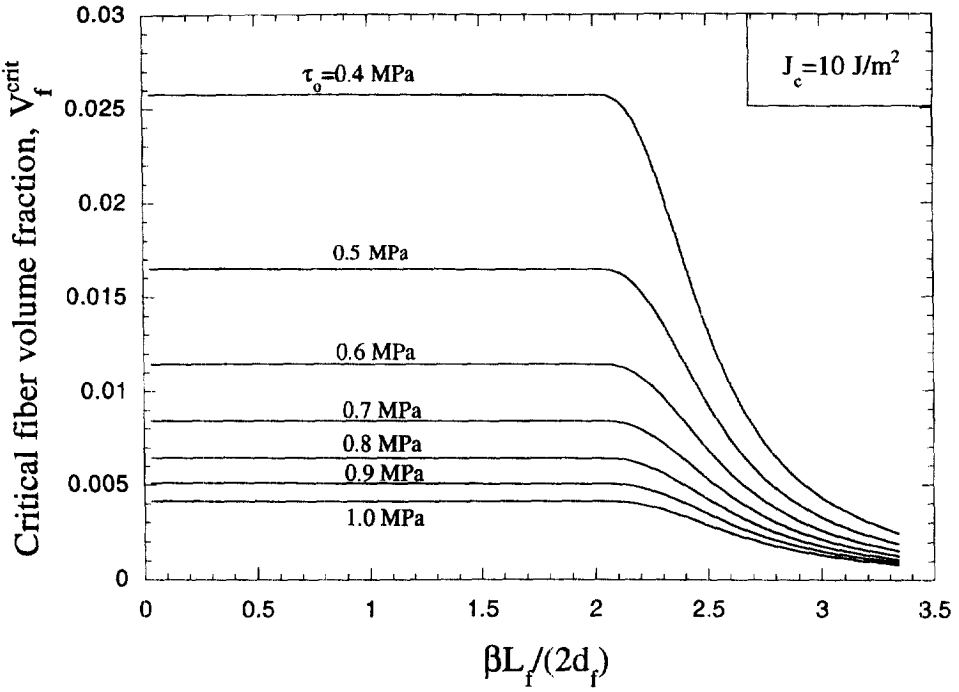

Fig. 8. Critical fiber volume fraction for multiple cracking as a function of interface properties τ_0 and β with all other parameters fixed for a Spectra-900 fiber(untreated)/cement composite (L_f = 12.7 mm, d_f = 38 μm, E_f = 117 GPa).

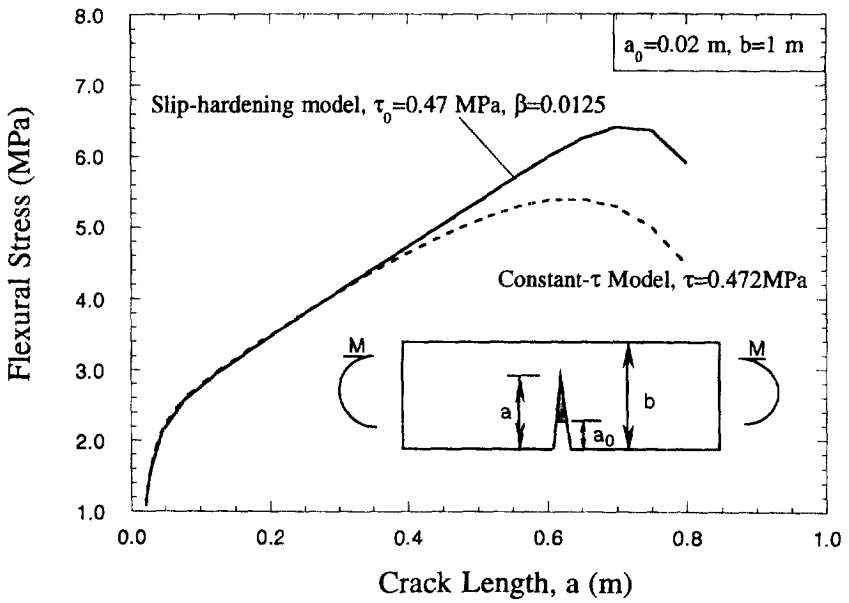

Fig. 9. Comparison of flexural stress versus equilibrium crack length relation of a pre-cracked beam predicted by the present slip-hardening crack bridging model to that predicted using the constant-τ model.

opening become large, bridging stress level is maintained or even increased by slip-hardening effect while it drops in constant-τ model, and two curves start to deviate. In conclusion, slip-hardening at interface also increases the load carrying capacity of a composite structure member in the case of fiber pullout (no fiber rupture occurs).

7. CONCLUSIONS AND DISCUSSIONS

Slip-hardening interface behavior has been commonly observed in synthetic fiber/cement matrix systems mainly due to fiber surface abrasion. In the present study, a new parameter β is introduced into the interface constitutive relation to take into account the slip-hardening effect on interface shear stress. A micromechanics-based single fiber pullout P–δ relation is theoretically constructed and shown to be quite accurate and robust in describing the slip-hardening interface behavior. Furthermore, a new crack bridging law is developed for randomly oriented flexible fiber reinforced cementitious composites with slip-hardening interfaces. Based on the present crack bridging model, we can draw the following conclusions:

(1) There exists a critical condition which must be satisfied for slip-hardening interface shear stress to significantly influence the composite properties. This condition is theoretically derived to be $\beta L_f/2d_f > 2$.

(2) For the material system satisfying the above-mentioned condition, slip-hardening interface shear stress can significantly increase the ultimate strain capacity and fracture energy due to fiber bridging while increase in composite tensile strength and flexural strength is less pronounced. Slip-hardening interface behavior also provides a possible way for further reducing material cost (through reducing critical fiber volume fraction) and maintaining sufficient ductility of the composite by ensuring multiple cracking (and hence strain-hardening). However, one has to sacrifice the composite tensile strength when fiber volume fraction becomes too low.

(3) The present micromechanical model provides a useful tool for material design for desired properties, especially for ductility in terms of both strain capacity and fracture toughness, by tailoring the interface properties.

With regard to the critical condition $\beta L_f/2d_f > 2$, it is desirable to use long and thin fibers. However, fiber length may be limited by workability during material processing and the possibility of rupture in service. Plasma treatment of the fiber seems to increase β as indicated in this work. Systematic study on the dependence of β has not yet been carried out and is certainly needed for interface property control. On the other hand, the present model has not taken into account the possibility of fiber rupture, which could be important if a low performance fiber is used.

It should be noted that the present refined fraction model is a direct extension of the MCE model (Marshall, Cox and Evans, 1985), in which the constant frictional stress is the only interface parameter to include the slip-hardening effect. There have been more sophisticated models that take into account the effects of fiber/matrix interface fracture toughness, Poisson contraction and residual stresses (e.g., Gao *et al.*, 1988; Hsueh, 1990; Hutchinson and Jensen, 1990). But none of these models could explain the post-debonding rising portion of the single fiber pullout curves as

shown in Fig. 5 without introducing a slip-hardening interface constitutive relation (e.g., eqn (2)). Since, after fully debonding, the interface fracture toughness becomes irrelevant, residual axial stress (if any) will be mostly released and Poisson's contraction does not give rise to slip-hardening behavior, it is necessary to introduce a relation between interface shear stress and fiber slippage as proposed in this study although it is a phenomenological one.

As far as the debonding process is concerned, interface fracture toughness, Poisson's effect and residual stresses are theoretically considered to be important factors. In a Coulomb friction model, the residual clamping stress and Poisson contraction result in a nonuniform friction stress distribution along a debonded interface and in some cases frictionless debonding (causing load drop), provided the fiber is perfectly aligned and with smooth surface. However, the experimental results of Baggott and Gandhi (1981) indicated that slight misalignment in the specimen and the asperities of the fiber surface could offset the Poisson's effect. The conclusion that the assumption of a constant frictional stress is appropriate when friction results from the interface roughness effect can also be found in Jero *et al.* (1991) and Mackin *et al.* (1992). Slight misalignment in a pull-out test (no alignment at all in a random short fiber reinforced cementitious composite) and rough interface are inevitable. Furthermore, no unstable load drop during debonding has been observed in previous pullout tests of commonly-used flexible synthetic fibers (e.g., nylon and polypropylene fibers (Wang *et al.*, 1988), which have relatively high Poisson's ratios). Thus, it follows that in general the Poisson's effect can be neglected and a one-dimensional model is usually adequate to describe the fiber pullout process in these fiber/cement systems. In such a constant friction stress model (e.g., Marshall *et al.*, 1985; Li, 1992), the effect of residual clamping stress should be reflected in the value of τ, which is determined from the first bend-over point (end of debonding) of a single fiber pullout curve if interface fracture toughness is neglected. The axial residual stress in the fiber is usually negligible due to the unique processing of cementitious composites in contrast to that of ceramic-based composites, in which thermal residual stresses can be significant.

With regard to the effect of interface fracture toughness, it does give rise to a higher debonding load and a subsequent load drop right after fully debonding (Gao *et al.*, 1988; Leung, 1992). Many kinds of polymeric fibers used in cement-based composites are of hydrophobic nature, including polyethylene and polypropylene fibers, which results in a very weak chemical bond with cement matrix (i.e., low interface fracture toughness) as evidenced by very little or no load drop after fully debonding (e.g., the polyethylene fiber cases shown in Fig. 5). Consequently, the interface fracture toughness in these fiber/cement matrix systems can be neglected. Surface treatment can somewhat increase chemical bonding, and fibers with hydrophilic nature such as polyvinyl-Alcohol (PVA) fibers can form strong chemical bonds with the cement matrix and can result in high interface fracture toughness. In such cases, the interface fracture toughness needs to be considered. Part of recent research results regarding this aspect is included in Appendix III (Lin and Li, 1996). It is clear that interface fracture toughness does not give rise to larger crack opening at maximum bridging stress. Instead, it shifts the peak of debonding stage σ_B–δ curve to the smaller crack opening end.

Based on the above considerations, we believe that the slip-hardening interface

behavior is the dominant mechanism behind the large discrepancy between experimental results and predictions with the constant friction model, which has already been proven to be a quite accurate model even in predicting the crack opening at maximum bridging stress for a Nylon fiber reinforced cement (Li and Maalej, 1996). The refinement added to this model by employing (2) has been shown to be satisfactory in explaining the discrepancy while other mechanisms are either negligible, such as Poisson's contraction and residual stresses, or cannot give rise to a resolution to the problem even if it is included (e.g., the interface fracture toughness).

ACKNOWLEDGEMENTS

This work has been supported by a grant from the National Science Foundation (MSS-9301949) to the ACE-MRL at the University of Michigan. Helpful discussions with T. Kanda, H. C. Wu and T. Matsumoto are gratefully acknowledged.

REFERENCES

Aveston, J., Cooper, G. A. and Kelly, A. (1971) Single and multiple fracture. In *The Properties of Fiber Composites*, Conf. Proc. National Physical Lab., pp. 15–26. IPC Science and Technology Press, Surrey, U.K.

Baggott, R. and Gandhi, D. (1981) Multiple cracking in aligned polypropylene fiber reinforced cement composites. *J. Mater. Sci.* **16**(1), 65–74.

Bao, G. and Song, Y. (1993) Crack bridging models for fiber composites with degraded interfaces. *J. Mech. Phys. Solids* **41**, 1425–1444.

Cox, B. N. and Marshall, D. B. (1991) Stable and unstable solutions for bridged cracks in various specimens. *Acta Metall. Mater.* **39**(4), 579–589.

Gao, Y.-C., Mai, Y.-W. and Cotterell, B. (1988) Fracture of fiber-reinforced materials. *J. Appl. Math. Phys.* **39**, 550–558.

Holmes, J. W. and Cho, C. (1992) Experimental observations of frictional heating in fiber-reinforced ceramics. *J. Am. Ceram. Soc.* **75**(4), 929–938.

Hsueh, C. H. (1990) Interfacial debonding and fiber pull-out stresses of fiber-reinforced composites. *Mater. Sci. Eng.* **A123**(1), 1–11.

Hsueh, C. H. (1996) Crack-wake interfacial debonding criteria for fiber-reinforced ceramic composites. *Acta Mater.* **44**(6), 2211–2216.

Hutchinson, J. W. and Jensen, H. M. (1990) Models of fiber debonding and pullout in brittle composites with friction. *Mech. Mater.* **9**, 139–163.

Jero, P. D., Kerans, R. J. and Parthasarthy, T. A. (1991) Effect of interfacial and roughness on the frictional stress measured using push-out tests. *J. Am. Ceram. Soc.* **74**(11), 2793.

Krenchel, H. and Hansen, S. (1987) Durability of polypropylene fibers in concrete. *Nordic Concrete Res.* **6**, 143–153.

Leung, C. K. Y. (1992) Fracture-based two-way debonding model for discontinuous fibers in elastic matrix. *J. Eng. Mech.* **118**(11), 2299–2317.

Li, V. C. (1992) Post-crack scaling relations for fiber reinforced cementitious composites. *ASCE J. Mater. Civil Engng* **4**(1), 41–57.

Li, V. C. (1993) From micromechanics to structural engineering—the design of cementitious composites for civil engineering applications. *JSCE J. of Struct. Mech. Earthquake Engng* **10**(2), 37–48.

Li, V. C. and Leung, C. K. Y. (1992) Steady state and multiple cracking of short random fiber composites. *ASCE J. Engng Mech.* **118**(11), 2246–2264.

Li, V. C. and Wu, H. C. (1992) Conditions for pseudo strain-hardening in fiber reinforced brittle matrix composites. *J. Appl. Mech. Rev.* **45**(8), 390–398.

Li, V. C. and Maalej, M. (1996) Toughening in cement based composites. Part II: Fiber reinforced cementitious composites. *Cement and Concrete Compos.* **18**(4), 239–249.
Li, V. C. and Stang, H. (1996) Interface property characterization and strengthening mechanisms in fiber reinforced cement based composites, submitted for publication in *J. Advanced Cement Based Composites*, UMCEE Report 96-1.
Li, V. C., Wang, Y. and Backer, S. (1990) Effect of inclining angle, bundling, and surface treatment on synthetic fiber pull-out from a cement matrix. *Composites* **21**(2), 132–140.
Li, V. C., Wang, Y. and Backer, S. (1991) A micromechanical model of tension softening and bridging toughening of short random fiber reinforced brittle matrix composites. *J. Mech. Phys. Solids* **39**(5), 607–625.
Li, V. C., Wu, H. C. and Chan, Y. W. (1995a) Interfacial property tailoring for pseudo strain-hardening cementitious composites. In *Advanced Technology on Design and Fabrication of Composite Materials and Structures* (eds Carpinteri and Sih), pp. 261–268.
Li, V. C., Mihashi, H., Wu, H. C., Alwan, J., Brincker, R., Horii, H., Leung, C., Maalej, M. and Stang H. (1995b) Micromechanical models of mechanical response of HPFRCC. In *High Performance Fiber Reinforced Cementitious Composites* (eds A. Naaman and H. Reinhatdt).
Li, V. C., Wu, H. C. and Chan, Y. W. (1996) Effect of plasma treatment of polyethylene fibers on interface and cementitious composite properties. *J. Amer. Ceram. Soc.*, accepted for publication.
Lin, Z. and Li, V. C. (1996) On interface property characterization and performance of fiber reinforced cementitious composites, manuscript in preparation.
Mackin, T. J., Warren, P. D. and Evans, A. G. (1992) Effect of fiber roughness on interface sliding in composites. *Acta. Metall. Mater.* **40**(6), 1251–1257.
Maalej, M., Hashida, T. and Li, V. C. (1995) Effect of fiber volume fraction on the off-crack-plane fracture energy. In strain-hardening engineered cementitious composites. *J. Am. Ceram. Soc.* **78**(12), 3369–3375.
Marshall, D. B., Cox, B. N. and Evans, A. G. (1985) The mechanics of matrix cracking in brittle-matrix fiber composites. *Acta Metall. Mater.* **33**, 2013–2021.
McCartney, L. N. (1987) Mechanics of matrix cracking in brittle matrix fiber-reinforced composites. *Proc. Roy. Soc. Lond.* **A409**, 329–350.
Morton, J. and Groves, G. W. (1976) The effect of metal wires on the fracture of a brittle matrix composite. *J. Mater. Sci.* **11**, 617–622.
Naaman, A. E. (1992) SIFCON: Tailored properties for structural performance. In *High Performance Fiber Reinforced Cement Composites* (eds H. W. Reinhardt and A. E. Naaman), pp. 18–38. E & FN Spon, London.
Shao, Y., Li, Z. and Shah, S. P. (1993) Matrix cracking and interface debonding in fiber-reinforced cement-matrix composites. *Advanced Cement Based Mater.* **1**, 55–66.
Wang, Y., Li, V. C. and Backer, S. (1988) Modeling of fiber pull-out from a cement matrix. *Int. J. Cement Compos. Lightweight Concrete* **10**(3), 143–149.
Wu, H. C. and Li, V. C. (1992) Snubbing and bundling effects on multiple crack spacing of discontinuous random fiber-reinforced brittle matrix composites. *J. Am. Ceram. Soc.* **75**(12), 3487–3489.
Wu, H. C. and Li, V. C. (1995) Stochastic process of multiple cracking in discontinuous random fiber reinforced brittle matrix composites. *Int. J. Damage Mech.* **4**(1), 83–102.
Yang, J. M., Jeng, S. M. and Yang, C. J. (1991) Fracture mechanisms of fiber-reinforced titanium alloy matrix composites. Part I: Interfacial behavior. *Mater. Sci. Engng* **A138**, 155–167.

APPENDIX I

I.1. Derivation of debonding stage P–δ *relation*

Following Marshall *et al.* (1985) and Bao and Song (1993), consider the cylindrical model depicted in Fig. 4. In the bonded zone, the compatibility condition requires that the axial strain in the fiber ε_f and that in the matrix ε_m be the same, i.e.,

$$\varepsilon_f = \varepsilon_m. \tag{I.1}$$

Neglecting Poisson's effect, we have in the bonded region

$$\frac{\sigma_f}{E_f} = \frac{\sigma_m}{E_m} \tag{I.2}$$

where σ_f and σ_m are the stress in the fiber and in the matrix, respectively. Balance of axial forces in the matrix and the fiber gives

$$\sigma_m = -\frac{\pi d_f \ell \bar{\tau}}{A_m} \tag{I.3}$$

and

$$\sigma_f = \frac{P - \pi d_f \ell \bar{\tau}}{A_f} \tag{I.4}$$

where A_f and A_m are the cross-section area of the fiber and the matrix shell respectively; ℓ is the debonded zone length and $\bar{\tau}$ is the average interfacial shear stress given by

$$\bar{\tau} = \frac{1}{\ell}\int_0^{\ell} \tau(z)\,dz. \tag{I.5}$$

We will derive the interfacial shear stress distribution $\tau(z)$ shortly. From (I.2), (I.3) and (I.4), we have

$$P = \pi d_f \ell \bar{\tau}(1+\eta) \tag{I.6}$$

with

$$\eta = \frac{V_f E_f}{V_m E_m}.$$

Define the interface slip as the (local) relative displacement between the fiber and the matrix, that is,

$$S(z) = u_f(z) - u_m(z). \tag{I.7}$$

Hence

$$\frac{dS}{dz} = \frac{du_f}{dz} - \frac{du_m}{dz} = \varepsilon_f(z) - \varepsilon_m(z). \tag{I.8}$$

Local equilibrium requires

$$\frac{d\sigma_f(z)}{dz} = \frac{4}{d_f}\tau(S) \quad \text{and} \quad \frac{d\sigma_m(z)}{dz} = -\frac{\pi d_f}{A_m}\tau(S). \tag{I.9}$$

Differentiating (I.8) and using $\varepsilon_f(z) = \sigma_f(z)/E_f$ and $\varepsilon_m(z) = \sigma_m(z)/E_m$, we obtain

$$\frac{d^2 S}{dz^2} = \frac{4(1+\eta)}{E_f d_f}\tau(S). \tag{I.10}$$

Using the interface constitutive relation (2) and recognizing the fact that at the tip of the debonding zone ($z = 0$), $u_f = u_m$ and $\varepsilon_f = \varepsilon_m$, we obtain the governing equations for this boundary value problem

$$\frac{d^2S}{dz^2} - \frac{\omega^2}{d_f^2} S = \frac{\omega^2}{\beta d_f} \tag{I.11}$$

and at $z = 0$,

$$S = 0 \quad \text{and} \quad dS/dz = 0 \tag{I.12}$$

where

$$\omega = \sqrt{\frac{4(1+\eta)\beta\tau_0}{E_f}}. \tag{I.13}$$

The solution to (I.11) and (I.12) can be found to be (Bao and Song, 1993)

$$S(z) = \frac{d_f}{\beta}[\cosh(\omega z/d_f) - 1] \quad \text{and} \quad \tau(z) = \tau_0 \cosh(\omega z/d_f). \tag{I.14}$$

From (I.5), (I.6) and (I.14), we obtain the relation between applied load P and debonding length ℓ

$$P = \frac{\pi d_f^2 \tau_0 (1+\eta)}{\omega} \sinh(\omega \ell/d_f). \tag{I.15}$$

The fiber end slippage distance is given by

$$u = S(z = \ell) = \frac{d_f}{\beta}[\cosh(\omega \ell/d_f) - 1]. \tag{I.16}$$

The corresponding crack opening due to fiber sliding during debonding stage is given by $\delta = 2u$. Eliminating ℓ from (I.15) and (I.16) and assuming the present formulation is valid for up to full debonding length L, we have

$$P = \frac{\pi d_f^2 \tau_0 (1+\eta)}{\omega} \sqrt{\left(1 + \frac{\beta\delta}{2d_f}\right)^2 - 1}, \quad \text{for } 0 \leqslant \delta \leqslant \delta_0 \tag{I.17}$$

where

$$\delta_0 = \frac{2d_f}{\beta}[\cosh(\omega L/d_f) - 1]. \tag{I.18}$$

It can be shown that by taking limit analysis as $\beta \to 0$, (I.17) becomes identical to the constant-τ ($\tau = \tau_0$) model obtained by Marshall, Cox and Evans (1985).

I.2. Derivation of post-debonding (pullout) stage P–δ relation

During fiber pullout stage, by ignoring the fiber elastic stretch, the fiber/matrix slip distance S can be approximated as (Fig. 4(b))

$$S = \frac{d_f}{\beta}[\cosh(\omega z/d_f) - 1] + (\delta - \delta_0). \tag{I.19}$$

The first term in (I.19) is the slip distribution at full debonding and the second term is due to the uniform slip of the 'frozen' fiber. The interfacial shear stress is then given by the constitutive relation $\tau = \tau_0 (1 + \beta S/d_f)$ and the pullout load can be approximated by

$$P = \pi d_f (1+\eta) \int_{\delta - \delta_0}^{L} \tau(z)\,\mathrm{d}z \tag{I.20}$$

and (4) yields

$$P = \frac{\pi d_f^2 \tau_0 (1+\eta)}{\omega}\left[\sinh\left(\frac{\omega L}{d_f}\right) - \sinh\left(\frac{\omega(\delta-\delta_0)}{d_f}\right)\right] + \pi\tau_0\beta(1+\eta)(\delta-\delta_0)(L-(\delta-\delta_0)).$$

It should be noted that the above P–δ relation is based on one-sided pullout assumption which is valid for non-slip-hardening cases. In the case of slip-hardening, because of the load increase in the fiber due to the pullout of the shorter embedded fiber segment, the longer embedded fiber segment may reach complete debonding stage and a two-sided pullout scenario may happen (Li *et al.*, 1990). It can be shown that for two-sided pullout to occur, the shorter fiber embedment length L_1 should satisfy the following condition:

$$\frac{L_f}{2} \geqslant L_1 \geqslant \left[\frac{2+(1+c\tilde{\delta})\tilde{\delta}}{2+c\tilde{\delta}}\right]\frac{L_f}{2}, \quad \text{with } c = \frac{\beta L_f}{2d_f} \quad \text{and} \quad \tilde{\delta} = \delta/(L_f/2). \tag{I.21}$$

Practically, the crack opening is on the order of sub-millimeter ($\tilde{\delta} \sim 10^{-2}$) and c is of order 1. Therefore, only those fibers with shorter embedment length L_1 very close to $L_f/2$ will have the possibility to undergo two-sided pullout. In the case of completely random fiber distribution, the fiber population satisfying (I.21) is expected to be small so that the effect of two-sided pullout is negligible.

APPENDIX II

II.1 Derivation of pre-debonding σ_B–δ relation (8a)

Equation (7) in main text can be rewritten in the following

$$\tilde{\sigma}_B = \frac{\sigma_B}{\sigma_1} = \frac{8}{\pi\tau_0(L_f/d_f)d_f^2}\int_{\phi=0}^{\pi/2}\int_{z'=0}^{\cos\phi} P(\delta)\sin\phi\,\mathrm{d}z'\,\mathrm{d}\phi \tag{II.1}$$

with

$$\sigma_1 = \tfrac{1}{2}\tau_0 V_f (L_f/d_f) \quad \text{and} \quad z' = z/(L_f/2). \tag{II.2}$$

For the pre-debonding σ_B–δ curve, there are two contributions from individual fibers. For those fibers located or oriented in such a way as to have a long embedment length L, their contributions are through fiber debonding, as described by (3). For the other fibers, their contributions are through fiber slipping, as described by (4). Fibers in the first group pass into the second group as δ increases. For the first group of fibers, it is important to recognize that (3) holds as long as

$$\delta < \delta_0 = \frac{2d_f}{\beta}[\cosh(\omega L/d_f) - 1] \tag{II.3}$$

and the fiber embedment length L can be re-expressed in terms of the fiber length L_f, the centroidal location z, and orientation angle ϕ of the particular fiber as

$$L = \frac{L_f}{2} - \frac{z}{\cos\phi}. \tag{II.4}$$

After transformation and normalization, (II.3) becomes

$$z' < z_0 \cos\phi, \quad \text{with } z_0 = 1 - \frac{1}{k}\cosh^{-1}\left(1 + \frac{\beta\delta}{2d_f}\right) \quad \text{and} \quad k = \frac{\omega L_f}{2d_f}. \tag{II.5}$$

Thus, for this group of fibers, the contribution to the bridging stress is given by

$$\tilde{\sigma}_B(\delta)|_{\text{debonding}} = \frac{8}{\pi\tau_0(L_f/d_f)d_f^2}\int_{\phi=0}^{\pi/2}\int_{z'=0}^{z_0\cos\phi} P(\delta)\sin\phi\,dz'\,d\phi \tag{II.6}$$

with $P(\delta)$ given by (3). The upper integration limit for z' in (II.6) ensures that only those fibers not fully debonded are counted in this contribution.

For the second group of fibers, slipping occurs, and (4) holds as long as

$$\delta_0 < \delta \leqslant L = \frac{L_f}{2} - \frac{z}{\cos\phi} \tag{II.7}$$

i.e.

$$z_0\cos\phi < z' \leqslant (1-\tilde{\delta})\cos\phi. \tag{II.8}$$

Thus for this group of fibers, the contribution to the bridging stress is given by

$$\tilde{\sigma}_B(\delta)|_{\text{slipping}} = \frac{8}{\pi\tau_0(L_f/d_f)d_f^2}\int_{\phi=0}^{\pi/2}\int_{z'=z_0\cos\phi}^{(1-\tilde{\delta})\cos\phi} P(\delta)\sin\phi\,dz'\,d\phi \tag{II.9}$$

with $P(\delta)$ given by (4). The lower integration limit for z' in (II.9) ensures that only those fibers fully debonded are counted in this contribution, and the upper integration limit ensures that those fibers that have fully slipped out of the matrix play no further role in the bridging stress.

By combining these two contributions for any given $\delta < \delta^*$, we obtain

$$\begin{aligned}\tilde{\sigma}_B(\delta) &= \tilde{\sigma}_B(\delta)|_{\text{debonding}} + \tilde{\sigma}_B(\delta)|_{\text{slipping}} \\ &= \frac{2g(1+\eta)}{k}\left[1 - \frac{1}{k}\cosh^{-1}\left(1+\frac{\beta\delta}{2d_f}\right)\right]\sqrt{\left(1+\frac{\beta\delta}{2d_f}\right)^2 - 1} + g(1+\eta)\frac{\beta\tilde{\delta}}{\omega k}.\end{aligned} \tag{II.10}$$

By using the normalization factors defined in main text, (II.10) results in the first equation in (8). In deriving (II.10), the condition $k\tilde{\delta} \ll 1$ is used to simplify the results and those terms involving $\tilde{\delta}^2$ resulting from (II.9) are dropped without loss of accuracy.

II.2. Derivation of post-debonding σ_B–δ relation (8b)

We recognize that for $\delta > \delta^*$, all fibers would be slipping. Again, starting from (7) or (II.1), and eliminating all fibers that have fully slipped out from the matrix, the bridging stress may be written as

$$\tilde{\sigma}_B(\delta)|_{\text{slipping}} = \frac{8}{\pi\tau_0(L_f/d_f)d_f^2}\int_{\phi=0}^{\pi/2}\int_{z'=0}^{(1-\tilde{\delta})\cos\phi} P(\delta)\sin\phi\,dz'\,d\phi \tag{II.11}$$

where the fiber bridging force is given by (4). After rather tedious derivation, we arrive at a simple expression

$$\tilde{\sigma}_B(\delta) = g(1+\eta)\left(1 + \frac{\beta L_f}{2d_f}\tilde{\delta}\right)(1-\tilde{\delta})^2. \tag{II.12}$$

Again, in evaluating (II.11), $k\tilde{\delta} \ll 1$ is used to simplify the results without loss of accuracy.

APPENDIX III

III.1. Effect of interface fracture toughness on debonding stage σ_B–δ relation

For clarity and without loss of accuracy, the slip-hardening effect during fiber debonding stage will be neglected. Based on the energy-based criterion (e.g., Gao *et al.*, 1988; Hsueh, 1996), it can be shown that the P–δ relation is given by (Lin and Li, 1996)

$$P = \frac{\pi d_f^2}{4}\sqrt{\frac{4(1+\eta)E_f\tau_0\delta}{d_f} + \frac{8G_dE_f(1+\eta)}{d_f}} \tag{III.1}$$

where G_d is the interface fracture energy. Following the derivation outlined in Appendix II and assuming no fiber rupture, the crack bridging law for debonding stage can be obtained as follows

$$\frac{\sigma_B}{\sigma_0} = \sqrt{4\frac{\delta}{\delta_0^*} + \gamma^2} - \frac{\delta}{\delta_0^*}, \quad \text{for } 0 \leqslant \delta \leqslant \delta_0^*(1+\gamma) \tag{III.2}$$

where

$$\gamma = \sqrt{\frac{8G_d}{\tau_0\delta_0^*}}, \quad \sigma_0 = \frac{1}{2}gV_f\tau_0L_f/d_f$$

and

$$\delta_0^* = \frac{\tau_0L_f^2}{E_fd_f(1+\eta)}$$

which is the same as the crack opening corresponding to maximum bridging stress given by the constant friction stress model ($G_d = 0$).

It is easy to find out that the crack opening corresponding to the maximum bridging stress is given by

$$\delta = \left(1 - \frac{\gamma^2}{4}\right)\delta_0^* \tag{III.3}$$

which is less than δ_0^* predicted by the constant friction stress model with zero interface fracture energy. Therefore, the interface fracture toughness does not give rise to larger crack opening at maximum bridging stress if the post-debonding slip-hardening behavior is not considered.